La-Ag-Co perovskites for the catalytic flameless combustion of methane

O. Buchneva[a], I. Rossetti[a*],C. Biffi[a], M. Allieta[a], A. Kryukov,[b] N. Lebedeva.[b]

[a)] Dip. Chimica Fisica ed Elettrochimica, Università di Milano, v. C. Golgi, 19, 20133 Milano, Italy

[b)] Dip. of Physical Chemistry, Mendeleev's University of Chemical Technology od Russia, Miusskaya sq. 9. 125047, Moscow, Russia

ABSTRACT

Ag represents an interesting dopant for the highly active $LaCoO_3$ perovskites used for the catalytic flameless combustion (CFC) of methane, due to its ability to adsorb and activate oxygen and to the possibility of incorporation into the framework as Ag^+ or Ag^{2+}, with formation of oxygen vacancies. In the present work we compared the catalytic activity and resistance to sulphur poisoning of a series of $LaCoO_3$, x%Ag/$LaCoO_3$, $La_{1-x}Ag_xCoO_3$ samples (nominal composition), the latter two notations indicating post synthesis Ag loading or direct incorporation during the synthesis, respectively. The samples were prepared by flame pyrolysis (FP) and by the sol gel (SG) method, leading to different particle size and possibly to different incorporation degree of the dopant, quantified by Rietveld refinement of XRD patterns.

Higher activity was observed, in general, with fresh catalysts synthesised by FP. The SG samples demonstrated a slightly better resistance to sulphur poisoning when considering the conversion decrease between the fresh and the poisoned samples, due to lower surface exposure. However, interesting data have been

* Corresponding author: ilenia.rossetti@unimi.it

obtained with some of the Ag-doped poisoned FP samples, performing even better than the fresh SG prepared ones.

Ag addition led to a complex change of activity and resistance to poisoning. The activity of FP prepared samples doped with a small amount of Ag (*e.g*. 5 mol%) was indeed lower than that of the undoped $LaCoO_3$. By contrast, a further increase of Ag concentration led to increasing catalytic activity, mainly when big extraframework Ag particles were present. By contrast, for SG samples a low Ag amount was beneficial for activity, due to an incresed reducibility of Co^{3+}.

Keywords: Catalytic combustion; Sulphur poisoning; Perovskite; Ag doping.

1 - INTRODUCTION

The catalytic flameless combustion (CFC) of methane allows to decrease the emission of nitrogen oxides, which usually form during high-temperature combustion in heat power plants [1,2]. Furthermore, this process relates with real possibility of energy production through utilisation of methane formed in ventilation emissions from coal mines. Perovskites show a catalytic activity for such application often comparable with that of supported noble metal-based catalysts. Together with a lower price, this makes perovskites promising catalysts for methane combustion, especially when suitable thermal and chemical stability is ensured by proper formulation and synthesis procedure. During the last years Ag-substituted perovskites were investigated. In particular, it was found that the introduction of Ag (10-30 mol%) in the structure of $LaMnO_3$ [3-5], $LaFeO_3$, $LaFe_{0.5}Co_{0.5}O_3$ [6] and $LaCoO_3$ [7] led to increasing activity with respect to unsubstituted samples. Song *et al.* [3] showed that for $LaMnO_3$ partial substitution of Ag and Sr for La led to increasing activity, following the scale M=Ce<La<Sr<Ag for $La_{0.7}M_{0.3}MnO_3$ samples.

Machocki *et al.* [4] explained that in the presence of silver the Mn-O bond strength is weakened, leading to easier Mn reduction to its lowest valence state and decreasing the temperature of transition from the suprafacial to the intrafacial mechanism [8], *i.e.* making easier the contribution of the bulk oxygen. Indeed, the formation of structure defects induced by the partial substitution increases oxygen mobility through the lattice. For silver substituted $LaFeO_3$ [6], an improvement of catalytic activity was also due to the intrinsic activity of metallic silver.

One of the key problems dealing with catalytic conversion of natural gas is the presence of sulphur compounds, added as odorisers in the distribution grid, possibly leading to catalyst poisoning. Voorhoeve *et al.* [9] found that 50 ppm SO_2 at 455°C caused a dramatic reduction of activity with Ba_2CoWO_6 and Ba_2FeNbO_6 for both CO oxidation and NO_x reduction. Furthermore, Li *et al.* [10] studied poisoning by SO_2 of $La_{1-x}A_xMnO_3$, where A=Sr, Ba, Ca and Pb, x=0.3 or 0.5, showing that these catalysts were severely and irreversibly poisoned by 50 ppm SO_2 at 240-300°C. Tejuka *et al.* [11] confirmed the dramatic decrease of methane oxidation rate in presence of small amounts of SO_2.

The poisoning mechanism can be explained by the absorption of SO_2 on the catalytically active B-sites leading to the formation of different sulphur-containing species. Based on the temperature and the composition of the catalyst, the following species: SO_2, SO_3, SO_3^{2-}, SO_4^{2-} and S^{2-}, have been reported [12]. In addition, prolonged exposure to SO_2 can lead to a complete destruction of the perovskite structure. Doping with noble metals or the introduction of transition metal ions forming unstable sulfates (*e.g.* Ti, Zr, V, Sn, Sr, Ce) in catalyst formulation are possible means to improve the resistance to sulphur poisoning. Rosso *et al.* [13-15] also showed the beneficial role of MgO, which acts as a protective shield, forming stable sulphates and hence competing with the active phase for SO_2 adsorption. Its

protective action is necessarily time-limited by its consumption. In a previous investigation [16] intra-framework Sr doping proved an interesting mean to improve catalyst resistance to poisoning, as well as the addition of noble metals, such as Pd or Pt. However, at least the former method showed beneficial for $LaMnO_3$ based catalysts, whereas $LaCoO_3$ showed decreasing activity upon Sr addition, besides being intrinsically less resistant to S poisoning. Based on this, we here propose $LaCoO_3$ doping with Ag ions, either partially inserted into the lattice or loaded after synthesis. Indeed, Ag is able to form stable S-based compounds and it shows an interesting activity for the title reaction. Furthermore, it has been shown in a previous investigation that it can be stabilised in unusual oxidation state (Ag^{2+}) in the framework of the $SrTiO_3$ perovskite [17,18].

Moreover, up to now there is no uniform theory on the relationship between composition, physical properties of the perovskite catalysts and resistance to sulphur compounds. Based on the above summarised topics, S-poisoning begins with SO_2 adsorption on oxygen vacancies and it is essentially a surface-based mechanism. Therefore, catalyst nanostructuring, besides affecting catalytic activity, can also deeply influence the resistance towards S-containing impurities. Recently in our laboratory we set up and optimised a flame pyrolysis (FP) method, already validated for the synthesis of widely different catalysts, many of which with perovskite like structure [19-24]. It is a one-step, continuous process, which allows to obtain single or mixed oxides with good phase purity and nanometric particle size. In addition, the high temperature of the flame ensures sufficient thermal stability, an aspect of paramount importance for the proposed application [22-24].

Therefore, in the present work we prepared a set of samples by two different procedures, namely FP and a modified citric acid method (SG). Catalysts with nominal composition $La_{1-x}Ag_xCoO_3$ with x=0, 0.05, 0.1, 0.2, were compared with

x%Ag/$LaCoO_3$ with x=2, 5, 10, prepared by post-synthesis doping with silver. The catalysts were tested for the CFC of methane, continuously monitoring their activity by on-line mass spectrometry. Resistance toward sulphur poisoning was checked by determining the residual activity after pulsed injections of tetrahydrotiophene (THT), a common odorising agent used in the natural gas grid. The effect of catalyst composition, preparation method and, consequently, nanostructuring on activity and stability have been investigated.

2 – EXPERIMENTAL

2.1 - Catalysts preparation

A series of perovskite-like samples with nominal composition $La_{1-x}Ag_xCoO_3$ with x=0, 0.05, 0.1, 0.2 were prepared by flame pyrolysis (FP) and by a modified version of the so-called sol-gel “citrate method” (SG) following the procedures below described. It is worth mentioning here that poor Ag incorporation in the $LaCoO_3$ is usually reached (*vide infra*). Therefore, the formula $La_{1-x}Ag_xCoO_3$ should be better represented by y-Ag/$La_{1-x-y}Ag_xCoO_3$, where x represents Ag incorporated into the lattice, y the molar fraction in extraframework position. However, to avoid complex notations, the nominal composition will be used in the following.

2.1.1 - Flame pyrolysis

All the precursors solutions were prepared by dissolving in propionic acid (Aldrich, pur. 97%) salts of the selected metals $La(CH_3COO)_3{\cdot}2H_2O$ (Aldrich, pur. 99.9%), $Co(CH_3COO)_2{\cdot}4H_2O$ (Fluka, pur. 99%), $Ag(CH_3COO)$ in the desired ratio and

metal concentration. The FP apparatus has been described in detail elsewhere [22]. Briefly, it consists of a capillary tube (inner diameter 0.6 mm) ending in the centre of a vertical nozzle and connected with a syringe pump (Harvard, mod. 975), feeding the solution of the mixed oxide precursors. The nozzle was co-fed with oxygen (SIAD, pur.>99.95%, flow rate 5 L/min), acting both as oxidant and as dispersing agent, able to form micro-droplets of solution. Gas flow rate was regulated by MKS (mod. 1259C) mass flow meters, controlled by a MKS (mod. 247C) control unit. The synthesized nano-particles were collected by means of a 10 kV electrostatic precipitator.

2.1.2 - Sol-gel method

Appropriate amounts of $La(NO_3)_3*6H_2O$ (ChemSpectr, pur. >98%), $Co(NO_3)_2*6H_2O$ (Reachem, pur. >98%) and $AgNO_3$ (Reachem, pur. 99.95%) were dissolved in a small amount of distilled water. Citric acid (Reachem, pur. 99.9%) was added to the solution as complexing agent with a 1.5:1 molar ratio with respect to the sum of metal cations. After evaporation of the solvent, a bulk powder was obtained, which was consecutively ignited at 300°C for 1h and at 550°C and 700°C for 3h (sample S0, Table 1).

For the preparation of post-synthesis Ag-doped catalysts (x%Ag/$LaCoO_3$ with x=2, 5, 10), $LaCoO_3$ was suspended in a concentrated solution of $AgNO_3$, containing 2, 5 or 10 mol% of $AgNO_3$ with respect to $LaCoO_3$. After drying of the suspension at 100°C, the powder was grinded in agate mortar and ignited at 650°C for 1h.

2.1.3 - Modified sol-gel method

After evaporation of the precursors solution, prepared as described in paragraph 2.1.2, at 80°C and drying at 150°C, a bulk powder was obtained, subsequently decomposed at 400°C for 1h and ground in plastic containers with a vibrating mill (MLW Thyr 2) for 1h. Grinding was carried out with steel balls (diameter 5-12mm) in hexane (hexane : powder = 12-15 vol/vol). After filtration and drying at 100°C, a portion of the powder was ignited at 700°C for 1h (sample S1) and another part (sample S2) was ignited at 550°C followed by repeated grinding (2h as described). Final thermal treatment of sample S2 was carried out at 650°C for 2h.

2.2 - Catalyst characterisation

The crystal structure of the prepared samples was determined by X-ray powder diffractometry on a Philips PW3020 diffractometer for the FP-samples and with “ДРОН-3”-difractometer for the SG-samples. The patterns obtained were compared with literature data for phase recognition [25]. The surface area of the synthesized powders was measured by N_2 adsorption/desorption at 77 K on a Micromeritics ASAP2010 apparatus, after outgassing at 300°C overnight. Scanning electron miscoscopy (SEM) analysis was carried out on a LEICA LEO 1420 instrument. The elemental composition of the catalysts has been checked by EDX analysis, confirming the nominal one within the experimental error (4.1%), calculated by comparison of different spot analyses on the same sample. The main properties of the prepared catalysts are summarised in Table 1.

2.3 – Catalytic activity testing

Catalytic activity tests were carried out by means of a continuous quartz tubular reactor on *ca.* 0.15 g of catalyst, pelletised, ground and sieved to 0.15-0.25 mm particles. Prior to each run, the catalyst was activated in flowing air (20 cm^3/min), while increasing temperature by 10°C/min up to 600°C, then kept for 1 h. The activity tests were carried out by feeding a mixture composed of 0.34 vol% CH_4, 33.3 vol% air, He balance, while increasing temperature by 10°C/min from 200°C up to 600°C. Gas flow rate was regulated by means of mass flowmeters (Brooks Instruments, mod. 5850) governed by a control unit (Brooks, mod. 0154). The total gas flow rate was 30 ml/min. The outcoming gas was analysed in line by means of a quadrupolar mass spectrometer (MKS, PPT Residual Gas Analyzer), selecting proper mass fragments.

Catalyst poisoning [16] was done in the same apparatus at 450°C by injecting 4 doses of 0.15 mg of tetrahydrothiophene (THT, Fluka, pur. >97%) per 1g of catalyst, each group of four injections being defined as cycle (corresponding to 0.6 mg THT per g of catalyst). The catalytic activity was monitored *"in operando"* during poisoning, by continuously analysing the relevant mass fragments (CH_4, THT, SO_2, SO_3, CO, CO_2, H_2O) and plotting them as partial pressure versus time. The data have been further elaborated by calculating the slope of some descriptive lines, indicating the transient response of the catalyst during poisoning, as better detailed in the result and discussion section. The standard activity test was then repeated after each poisoning cycle.

Temperature programmed desorption of oxygen (O_2 – TPD) was carried out on ca. 0.15 g of catalyst, pretreated in He (40 cm^3/min) from room temperature up to 800°C (10°C/min) and kept for 1h, then presaturated by oxygen in air flow at 750°C for 1h. The TPD curve was recorded by mass-spectrometry in the same conditions of the pretreatment. Temperature programmed reduction (TPR) was carried out after

the same pretreatment and saturation, by flowing 40 cm^3/min of 10 vol% H_2 in He gas mixture and by increasing temperature from r.t. up to 800°C by 10°C/min.

3 – RESULTS AND DISCUSSION

3.1 - Catalysts characterisation

According to the XRD data (Fig. 1 *a-c*) for all the samples the main phase is rhombohedral $LaCoO_3$ (characterised by a double reflection at $2\theta \approx 33°$). Typically, the reflections of metallic silver were also observed for doped samples ($2\theta \approx 38.1°$, 44.6° and 64.6°, empty squares), whose intensity increased with increasing Ag loading. This confirms the low Ag incorporation in the $LaCoO_3$ framework [4,5]. Due to poor silver solubility, the parameters of perovskitic lattice did not change dramatically, *i.e*. no relevant shift of the maximum reflection was observed for Ag-doped samples when compared with $LaCoO_3$.

Based on XRD patterns the average crystal size was calculated with the Scherrer equation $D = \frac{0.9 \cdot \lambda \cdot 180}{B \cdot \cos\theta \cdot \pi \cdot 10}$, where D (nm) is the average crystal size, λ (Å) the wavelength of the X-ray emitter, $B = \sqrt{FWHM^2 - 0.25^2}$, FWHM is the full reflection width at half maximum. The peak at $2\theta \approx 47°$ was chosen as reference. The results for every sample are shown in Table 1.

The average crystal size for x%Ag/$LaCoO_3$ samples was lower than for $La_{1-x}Ag_xCoO_3$, remaining comparable with the $LaCoO_3$ – SG0 starting material. A decrease of crystal size was achieved with the modified sol-gel procedure. Silver doping led to opposite effects on surface area for SG and FP samples. For SG catalysts silver doping brought about a slight decrease of specific surface area and increase of crystal size (Table 1), likely due to silver segregation as separate phase.

In case of post-synthesis deposition of silver followed by thermal treatment at 650°C this effect was less evident. By contrast, the FP technique is intrinsically characterised by a flash calcination, which limits any deep sintering of the powder, always leading to much higher surface area with respect to the homologous SG-prepared samples, as well as to smaller crystal size.

Structural parameters and mass fractions were obtained by Rietveld refinement, performed using the GSAS [26] software and its graphical interface EXPGUI [27]. The diffraction peak profiles have been fitted with a pseudo-Voight profile function. Only the perovskitic $LaCoO_3$ phase (rhombohedral system, space group *R*-3*c* [28]) was evident for x=0 both for FP and for SG samples. For x≥0.05 also the metallic Ag phase has been considered (cubic system, space group *Fm*-3*m*).

The Rietveld refinement relative to the undoped FP $LaCoO_3$ sample is shown in Fig. 2*a* as an example. A slight decrease of the calculated intensity has been identified with the broadening of X-ray reflections as a result of the presence of bimodal particles distribution in FP samples. Despite of this effect, adequate statistical parameters are generally obtained (wRp=0.0879, Rp=0.0680, $R(F^2)$= 0.0491, χ^2=1.031). These results have been adopted to estimate the incorporation degree of Ag. A first index is constituted by the variation of cell volume upon Ag doping. Unfortunately, due to the mentioned refinement problems for FP samples (reflection broadening, Co fluorescence and bimodal crystal size distribution), the error of the estimation of cell volume for FP samples was much higher than for SG samples. A decrease of the cell volume is observed when adding 5 and 10 mol% Ag, whereas non appreciable decrease of such parameter was attained by further Ag addition for FP samples. Similar conclusions can be drawn for SG samples with the exception of $La_{0.9}Ag_{0.1}CoO_3$. A better quantification of extraframework Ag has been achieved by considering the reflection of metallic Ag. By looking at the insert of Fig.

2*b*, one may notice a linear increase of the amount of segregated Ag when increasing its concentration. The FP and SG samples gave similar results, with a slightly lower Ag incorporation for the FP catalysts with respect to the SG ones. This is particularly relevant for the sample with nominal composition $La_{0.8}Ag_{0.2}CoO_3$. The amount of Ag incorporated into the framework can be estimated by difference from this value. A bit lower incorporation of Ag can therefore be concluded for FP samples with respect to SG, with a generally poor silver solubility in the $LaCoO_3$ lattice.

3.2 – Catalytic activity

All the catalysts exhibited a very high activity. Indeed, under the adopted reaction conditions full methane conversion was attained below 600°C and carbon dioxide + water were the only detected products. Mass spectrometric data showed sometimes a small drift of the baseline, which led to uncertain determination of T_0, *i.e.* the temperature at which methane conversion started. The activity curves were validated by analysing the effluent gas by gas-chromatography and the results were comparable within ±10°C. Furthermore, the experimental error of activity tests has been calculated on the basis of 4 repeated analyses, by comparing the conversion values at 450°C and resulted 7.1%.

The activity data collected on fresh SG-prepared sample are reported in Table 2 and Fig. 3. The modified sol-gel synthesis, *i.e*. additional milling of oxides in liquid phase did not lead to a significant increase of activity, nor of surface area (Tab.1), in spite of the slightly lower calcination temperature, which only decreased a bit crystal size (samples S1 and S2, Fig. 3). This is in line with the findings reported in [29], though contradicting some authors [30]. The higher activity of FP samples is correlated with their higher surface area, smaller crystal and particle size with respect to the SG homologues. This is not really relevant for surface exposition to reactants,

but we believe it is of paramount importance for oxygen mobility through the lattice. The intrafacial mechanism is indeed based on the latter parameter, as originally suggested by Voorhoeve [9]. The larger the crystal size, the longer is the pathway for oxygen from the bulk to the surface and vice versa. This is the reason why the catalytic activity of the FP prepared samples is always higher in spite of surface area depletion due to partial sintering under the activity testing conditions [22]. Indeed, characterisation of some spent samples, the FP-prepared $LaCoO_3$ and SG-synthesised $La_{0.8}Ag_{0.2}CoO_3$, showed that a similar surface area is obtained after the whole experimentation (4 m^2/g for the former and *ca*. 3 m^2/g for the latter).

In general, cation-substitution in the perovskite structure is an important instrument to modulate catalytic activity considering both the proposed reaction mechanisms [8]. For instance, the suprafacial mechanism can be affected by changing the electronic configuration of the d-element, also based on a possible synergistic effect due to combination of different elements at B position. By contrast, the intrafacial mechanism, can be improved by different type and concentration of lattice defects, in turn affecting oxygen mobility through the framework. However, the influence of the doping cations on catalytic activity depends on catalyst formulation and, at least to our knowledge, there is no consolidated theory really allowing to predict the influence of dopants.

In a previous investigation it was found [18] that in $Sr_{1-x}Ag_xTiO_{3\pm\delta}$ perovskites silver may exist as intra-crystalline framework Ag^{+2}, likely substituting part of Sr^{+2} in the lattice, and as inter-crystalline metallic silver. Ag^{+2} ions could interact with some O_x^- species, leading to O_x^-/Ag^{+2} couples and so influencing oxygen mobility and catalytic activity. However, it was found that a much lower Ag^{+2} substitution degree occurred for samples prepared by flame-based techniques (flame pyrolysis and flame hydrolysis [18]) with respect to the sol gel samples. This is very likely a consequence

of the milder sol-gel preparation conditions, allowing the perovskite lattice to allocate a higher amount of extraneous ions. As a vicar of the Sr^{+2} ion, the lattice Ag^{+2} ion is forced to assume this unusual charge by the perovskite crystal field force. Therefore, it is interesting to see whether it is possible to couple the beneficial effect of Ag doping with the intrinsically high activity of $LaCoO_3$. Indeed, silver substitution could end in Ag incorporation into the framework, in principle leading to an increased amount of defects in the framework, due to different ionic radius and lower valence of Ag with respect to La. Both these aspects could influence the mobility of lattice oxygen, which is the active factor for methane combustion in the high temperature region. In addition, metallic Ag deposition in extraframework position is also expected, mainly for FP-prepared samples, possibly showing its own catalytic contribution.

Partial substitution of Ag for La led to moderate contribution to activity in the case of sol-gel samples, an evident improvement of conversion appearing only at low Ag-loading. It is worth mentioning that an appreciable low temperature activity, leading to *ca*. 10% conversion below 350°C, appeared in the case of the SG prepared $La_{0.95}Ag_{0.05}CoO_3$ and $La_{0.8}Ag_{0.2}CoO_3$ catalysts, only. By looking at Fig. 2*b*, this can be explained by a higher variation of cell volume due to Ag incorporation for such samples with respect to $La_{0.9}Ag_{0.1}CoO_3$. To highlight this point, the cell volume of SG samples has been directly compared with catalyst conversion at 450°C, or better with (100-conv%): It immediately appears that with decreasing cell volume, i.e. with higher Ag incorporation into the framework, a higher activity is achieved (Fig. 4*a*). The same comparison for the FP samples led to an exactly opposite behaviour (Fig.4*b*), a higher incorporation into the framework provoking a decrease of catalytic activity.

To better quantify the activity trend, the kinetic constant was also calculated (Table 3), following the assumption of a first order reaction with respect to methane and pseudo-zero order with respect to oxygen, the latter being the excess reactant [31,32]. If the kinetic investigation is carried out in over-stoichiometric conditions (O_2/CH_4>5) and in the conversion range between 20% and 80%, the kinetic constant may be calculated as [33]:

$$k_m\left[\frac{\mu mole}{s \cdot g \cdot atm}\right] = \frac{V \cdot 1000}{V_m \cdot 60 \cdot m \cdot p} \ln\left(\frac{1}{1-\alpha}\right)$$

where V is the volumetric flow rate of the gas mixture (ml/min), V_m is the molar volume (l/mole), P the total pressure in the reactor (atm), α is methane conversion and *m* the mass of catalyst.

By comparing the kinetic constants of the undoped catalysts, one may notice that the FP sample doubles the value obtained with the SG one. Furthermore, the value calculated for the SG-prepared $La_{0.95}Ag_{0.05}CoO_3$ sample was approximately twice that of $LaCoO_3$ (sample S0, Table 3), however decreasing with further Ag addition. On this basis the activity of the SG samples show maximum activity for 5 mol% Ag doping, both when Ag is directly added during the preparation (Fig.5) or added after synthesis. By contrast, the FP samples showed an activity improvement only with 20 mol% Ag doping, lower silver addition inducing even negative effects on catalyst performance (Tables 2 and 3, Fig. 6). This can be explained as follows, separately considering the effect of intra- and extra-framework Ag.

The catalytic activity of Ag-based catalysts strongly depends on both oxidation state and particle size of silver. Studies of oxygen adsorption on Ag surfaces showed different forms of adsorbed oxygen [34]. Indeed, there is evidence of molecularly adsorbed oxygen at low temperature and of two kinds of adsorbed atomic oxygen species, occurring at higher temperature on single crystal (110) Ag surfaces [35,36].

Two types of atomic oxygen moieties, namely a chemisorbed surface atomic oxygen and subsurface oxygen, were identified as a result of dissociative oxygen adsorption on both single crystal (110) Ag surface and on polycrystalline Ag foils. Chemisorbed surface oxygen recombines and desorbs at *ca.* 320°C, whereas oxygen dissolution into the bulk starts at T>200°C. As a result of oxygen chemisorption at higher temperature and pressure, stable oxygen species are formed, which do not desorb below 520°C from the single crystal (110) surface. Therefore, the low activity of small Ag crystallites for the complete oxidation of methane may be interpreted in terms of oxygen adsorption. Anderson *et al*. [37] reported that the heat of oxygen adsorption on small Ag crystallites (3.7 nm) is 50 kcal/mol, much higher than the value relative to larger (27 nm) Ag crystallites. The heat of adsorption on big Ag crystallites was indeed close to what reported for single crystals (34÷41 kcal/mol). Therefore, small Ag crystallites lead to stronger Ag-O bond so decreasing the number of active sites for milder methane oxidation [38]. Silver particle size, calculated from XRD data with the Scherrer's equation (Table 1), showed that FP-$La_{0.8}Ag_{0.2}CoO_3$ contained approximately twice larger silver particles than FP-$La_{0.9}Ag_{0.1}CoO_3$. Of course, this estimate is rude, due to poor resolution of the reflection, but it explains the peculiar behaviour of FP samples: a higher segregation of Ag leads to bigger Ag particle size and hence to higher activity. When extra-framework Ag particle size is too low, it is not sufficiently active for this reaction. This effect is not evident for SG $La_{1-x}Ag_xCoO_3$ samples, though also in such case extraframework Ag is present. Metal crystal size (Table 1) is indeed generally lower for SG samples than for FP ones and this conclusion is corroborated by the slightly lower Ag segregation in extraframework position for the former catalysts (Fig.2*b*).

To better support the effect of extralattice Ag, the metal has been added post-synthesis to the S0 sample, always leading to an increase of catalytic activity (Tables

2 and 3, Fig. 7) in comparison with the SG prepared $LaCoO_3$ (S0). In particular, activity showed a maximum for sample 5%Ag/$LaCoO_3$. Silver crystal size has been estimated by XRD as 9.7nm for that sample. A much lower Ag dispersion, predominantly in extraframework position is indeed expected for this set of samples, though it cannot be completely excluded a minimal incorporation at the interface between the perovskite and the metallic cluster during the final calcination. Rietveld refinement of the metallic Ag phase allowed concluding that the whole Ag amount is in extralattice position. From all these data it is not surprising that maximum activity can be reached at relatively lower metal loading with respect to SG samples prepared by direct Ag incorporation.

Besides the intrinsic activity of extraframework Ag particles, it is interesting to check the effect of Ag incorporation into the lattice, though only partial.

As mentioned, also by taking into account the cell volume estimation error (Fig.2*b*) it is possible to consider significant the cell volume differences between the unsubstituted FP sample and the one containing nominally 5 and 10 mol% Ag. By contrast, no difference of cell volume can be observed when adding 20 mol% Ag. These results are confirmed by refining the metallic Ag profile, which leads to an estimation of segregated Ag amount (reported in Fig. 2b insert). By considering the full dots it is evident that the whole amount of Ag is segregated in extralattice position for the FP sample doped with 20 mol% Ag. *Ca*. one quarter of Ag added to the sample doped with 10 mol% Ag is in lattice position and *ca*. one fifth for the nominal $La_{0.95}Ag_{0.05}CoO_3$ catalyst. As for SG samples, a roughly constant Ag incorporation can be inferred, a bit higher than for FP samples only for the highest Ag amount.

Ag insertion into the lattice can bring about two effects. On one hand, it would induce an increase of oxygen vacancies concentration, due to its lower valence with respect to La. This can induce a higher oxygen mobility through the framework, but it

can also provoke a lower reducibility of Co^{3+}. The former phenomenon would increase catalytic activity, whereas the latter would induce the opposite effect.

The spontaneous release of oxygen can be monitored by TPD analysis of preadsorbed oxygen. A much more intense β peak was evident in the case of the undoped FP prepared $LaCoO_3$ sample, with respect to the Ag doped ones prepared by both methods. Furthermore, the peak onset was at *ca*. 733°C for the former and shifted towards higher temperature for the latter samples, reaching *e.g*. 750°C for catalyst FP-$La_{0.95}Ag_{0.05}CoO_3$, 760°C for catalyst SG-$La_{0.95}Ag_{0.05}CoO_3$ (value rather constant also for 760°C for catalyst SG-$La_{0.8}Ag_{0.2}CoO_3$) and a temperature higher than 800°C (experimental limit) for sample S0. This indicates that silver doped samples are less prone to oxygen release than the undoped one when prepared by FP, the opposite holding for the SG samples.

The same conclusion can be inferred when comparing the TPR patterns of the same catalysts (Fig. 8). The reduction temperature of Co^{3+} to Co^{2+}, represented by the first TPR feature, increased by *ca*. 50°C with the FP-prepared $La_{0.95}Ag_{0.05}CoO_{3-\delta}$ sample with respect to the undoped catalyst. By contrast, the SG-$LaCoO_3$ sample showed much less reducible than the FP one, Ag addition improving its reducibility. It is also worth noticing that samples $La_{0.95}Ag_{0.05}CoO_3$ are characterised by very similar TPR patterns and catalytic activity data.

As for catalytic activity, it can be concluded that with similar composition the FP prepared samples gave rise to a much higher catalytic activity with respect to the SG ones. The effect of Ag doping is complex and it leads to different results depending on the preparation procedure adopted. A summary of the possible effects of Ag on catalytic activity is drawn in scheme 1. Depending on the incorporation degree, oxygen vacancies may form, possibly leading to increased oxygen mobility (activity improvement), however accompanied by a decreased reducibility of Co

(slower redox cycle). Extralattice metallic silver may exploit a significant catalytic activity only when its dispersion is relatively low, since small Ag particles too strongly adsorbe oxygen. Therefore, Ag addition in low amount to SG-prepared cobaltite increases oxygen vacancies concentration improving oxygen mobility (lower β peak onset in TPD and higher Co reducibility in TPR analyses). Its effect is beneficial in improving the poor oxygen mobility through the lattice in a sample not very defective. By contrast, no significant effect of extraframework Ag is seen until big metallic particle size was reached by post synthesis Ag addition (lower dispersion). FP $LaCoO_3$ manifests by itself a very high Co reducibility and oxygen mobility if compared to SG samples. This is likely due to a very defective structure (bimodal crystal size distribution) and to very small crystal size, allowing a fast path for oxygen from the bulk to the surface and viceversa. Small Ag incorporation into the framework is useless in this case and it can even be detrimental inducing a lower Co reducibility and less spontaneous oxygen release (TPD-TPR). Only when proper big extraframework Ag particles are formed (comparable to post synthesis Ag doping of sample S0, but at much higher Ag loading), an activity improvement is seen due to the intrinsic catalytic activity of metallic Ag.,

3.3 Resistance to sulphur poisoning

Tetrahydrothiophene (THT) has been selected as poison due to its wide use as odorising agent in the methane distribution grid, where its concentration is *ca*. 8 ppmv. A detailed description of the testing procedure has been given elsewhere [16]. A preliminary set of experiments allowed concluding that THT instantly oxidised to SO_2, CO_2 and H_2O in the presence of the catalyst at the selected poisoning temperature, *i.e.* 450°C. This temperature has been chosen because most samples

exhibit the highest reaction rate around this value and the conversion curve is very steep, so the effect of poisoning can be magnified [16].

The activity tests on poisoned catalysts are reported in Fig.9-11. All samples lost part of their initial activity after poisoning as summarised in Table 2. According to the latter Table, sol-gel prepared samples seemed a bit more resistant to sulphur addition than the FP-synthesised ones. Indeed, when comparing the residual conversion at 450°C after THT injection, the SG samples lost in average one point % of conversion less than the FP samples (Table 2, column Δ%). The difference of conversion levels between the fresh and the poisoned samples increased with Ag loading, except for a minimum with $La_{0.9}Ag_{0.1}CoO_3$ for both the FP and SG preparation methods (-10/11 points%), up to 20 points% with the highest silver amount. It is worth noticing that when Ag is predominantly segregated, no significant difference of activity and resistance to sulphur poisoning can be observed between differently prepared samples, except for the contribution of the higher surface area and smaller crystal size of the FP-prepared samples. The relatively lower impact of the poison on SG-prepared samples can be explained on the basis of their lower surface area, since poisoning is commonly believed to start from SO_2 adsorption on the active sites, *i.e.* from a surface based interaction. Therefore, the lower surface area of SG catalysts exposes a lower amount of active sites for adsorption. The adsorbed SO_2 can react with oxygen forming surface sulphites or sulphates, which are stable below their decomposition temperature [10]. Reactive species (SO_2^-, SO^-) formed during adsorption are considered to react with surface oxygen of the perovskite to form SO_3^- radicals. It has also been reported [12] that some of the formed species are thermally unstable and react with oxygen (SO_4^-) or desorb at high temperature. Once formed, sulphur species may depress suprafacial activity [16] and bring about a less efficient intrafacial reactivity, due to a decreasing concentration of

available surface sites for oxygen release from the bulk. Their subsequent restoration through a Mars van Krevelen mechanism is inhibited too, for the same reasons. This activity depression should be evident until the decomposition temperature of sulphites and sulphates is reached (regeneration). However, sulphur species formation may also provoke the partial or total decomposition of the perovskite lattice, with a change of the cell parameters, thus leading to different oxygen mobility. When relevant, Ag incorporation into the framework may push part of cobalt ions to the highest valence state, increasing the acid character of the metal ion and therefore weakening the SO_2 bond with the surface. By contrast, when exposed on catalyst surface in oxidising atmosphere silver can also exploit the role of sulphur guard, protecting the adsorption sites by preferentially adsorbing S-containing poisons. However, it should be underlined by looking at the present data that Ag showed less effective than different dopants from the point of view of catalyst protection against poisoning. Indeed, no decrease of conversion has been observed when doping similar samples with Sr [16]. With the present Ag-doped samples the main advantage is the improved initial activity of some of them, which leads to satisfactory results even after more or less severe poisoning. Indeed, when the comparison between the activity on fresh and doped samples is carried out by considering the whole activity curve, one may observe that even after poisoning the FP prepared $La_{0.8}Ag_{0.2}CoO_3$ sample showed satisfactory activity, *e.g*. lower than the undoped FP prepared $LaCoO_3$, but higher than the SG prepared one, even when considering the fresh samples.

All the samples prepared by post synthesis Ag doping lost part of their initial activity after poisoning as it is pointed out in Table 2. The loss of conversion follows the catalytic activity scale. However, even for 5%Ag/$LaCoO_3$ which lost 20 points %

of initial activity (Table 2), residual conversion is still comparable with that of the fresh SG-prepared $LaCoO_3$ sample.

Therefore, it can be concluded that a sufficient amount of metallic Ag in extraframework position allows to protect the catalyst against poisoning, whereas, when it is incorporated into the lattice it leads to the formation of excess oxygen vacancies, which represent the first surface mean for adsorption of SO_x.

To check the effect of oxygen vacancies on the resistance towards sulphur poisoning, TPD experiments were carried out after activity and poisoning tests for some representative samples. The direct detection of SO_2 and SO_3 is not simple with MS, since their amount is very low and their signal is often lost in the background. A small and unquantifiable SO_2 desorption feature was observed starting from ca. 300°C with the FP-prepared $LaCoO_3$ sample. The same occurred with $La_{0.95}Ag_{0.05}CoO_3$ catalyst prepared by sol-gel, starting from ca. 250°C. Furthermore, by considering the TPD of oxygen of the same spent catalysts, a shift of the beta peak towards higher temperature was observed, indicating less easy oxygen release with respect to the fresh sample (*e.g.* 785°C for the spent SG-$La_{0.95}Ag_{0.05}CoO_3$, T > 800°C, limit of the experimental setting for FP-$LaCoO_3$).

3.4 Transient response

The trend of methane partial pressure *vs.* time during poisoning has been used to calculate an approximate deactivation rate at 450°C for every catalyst, as described elsewhere [16]. All the patterns have been approximated by straight lines and the corresponding slopes are reported in Table 4. The data there reported should be considered as an average poisoning rate. Negative values (usually very low) are connected with possible partial activity recovery in the whole poisoning cycle. For the first poisoning cycle the slope for FP samples was always higher than

for the SG catalysts with the same composition. Furthermore, for the FP samples the highest activity depletion was always observed during the first cycle (highest slope in Table 4). This confirms the importance of surface area exposure during poisoning. By contrast the SG catalysts were characterised by a highest slope of the transient response diagram for the second cycle, which means that they were sensitive to the addition of higher poison amounts (*e.g.* 1.2 mg of THT for two cycles). Post-synthesis Ag doping led to uniform poisoning in 2^{nd}-4^{th} cycles, but the role of the first cycle increased with increasing silver content.

From the transient response point of view $La_{0.8}Ag_{0.2}CoO_3$ showed the best catalysts irrespectively of the preparation route, since it was characterised by a minimum value of the mean deactivation rate and the pattern profile clearly showed progressive stabilisation. The worst behaviour was instead shown by SG samples with post-synthesis Ag deposition, because of progressively increasing mean deactivation rates (increasing with silver loading), with diverging profiles. By looking at residual conversion after the first and fourth poisoning cycle we can observe that samples functionalised post-synthesis showed the highest resistance upon the addition of low sulphur amounts. This is in line with the hypothesis of initial Ag surface coverage. However, Ag particles are less dispersed for these samples, with respect to *e.g.* $La_{0.8}Ag_{0.2}CoO_3$, which therefore offered a better overall resistance after further S addition due to higher Ag dispersion (Table 1).

4 – CONCLUSIONS

A set of silver doped La-Ag-Co-O samples has been prepared by different preparation methods, namely sol-gel and flame pyrolysis, leading to variable surface area and crystal size. The incorporation degree of the dopant was generally poor,

leaving extraframework metallic silver possibly showing its own catalytic activity, provided that proper Ag crystal size is reached. The effect of Ag doping on catalyst activity showed controversial, often increasing it in the case of SG prepared samples, especially in the case of post synthesis Ag addition.

Upon sulphur doping, a more or less evident conversion decrease was always observed, at difference with more suitable dopants from this point of view, such as Sr. A slightly higher poisoning effect was observed in the case of FP-prepared samples, likely due to their higher surface exposure. However, with proper formulation a satisfactory residual activity was attained with Ag doped samples, comparable with that of the fresh undoped ones.

REFERENCES

1. I. Rossetti, L. Forni, in “Synthesis, Properties and Applications of Oxide Nanomaterials”, J.A. Rodrìguez and M. Fernàndez-Garcìa, Eds., Wiley, 2007, 563-601.
2. R. Carroni, V. Schmidt, T. Griffin, Catal. Today, 75 (2002) 287-295.
3. K.-S. Song, H.X. Cui, S.D. Kim, S.-K. Kang., Catal. Today, 47 (1999) 155-160.
4. A. Machocki, T. Ioannides, B. Stasinska, W. Gac, G. Avgouropoulos, D. Delimaris, W. Grzegorczyk, S. Pasieczna, J. Catal., 227 (2004) 282-296.
5. B. Kucharczyk, W. Tylus, Appl. Catal. A: General, 335 (2008) 28-36.
6. V.R. Choudhary, B.S. Uphade, S.G. Pataskar, Fuel, 78 (1999) 919-921.
7. B. Kucharczyk, W. Tylus, Catal. Today, 90 (2004) 121-126.
8. R.J.H. Voorhoeve, J.P. Remeika, P.E. Freeland, B.T. Mathias, Science, 177 (1972) 353-354.
9. R.J.H. Voorhoeve, L.E. Trimble, C.P. Khattak, Mat. Res. Bull., 9 (1974) 655-666.
10. W. Li, in “Properties and applications of the Perovskite-type oxides”, G. Tejuca, J.L.G. Fierro (Eds.), Marcel Dekker, New York, 1993, 145-170.
11. L.G. Tejuca, J.L.G Fierro, J.M.D Tascón, Advances in Catal., 36 (1989) 237-328.

12. Y. Zhu, R. Tan, J. Feng, S. Ji, L. Cao, Appl. Catal. A: General, 209 (2001) 71-77.
13. I. Rosso, G. Saracco, V. Specchia, E. Garrone, Appl. Catal B: Environmental, 40 (2003) 195-205.
14. I. Rosso, E. Garrone, F. Geobaldo, B. Onida, G. Saracco, V. Specchia, Appl. Catal. B: Environmental, 34 (2001) 29-41.
15. I. Rosso, E. Garrone, F. Geobaldo, B. Onida, G. Saracco, V. Specchia, Appl. Catal. B: Environmental, 30 (2001) 61-73.
16. I. Rossetti, O. Buchneva, C. Biffi, R. Rizza, Appl. Catal. B: Environmental, 89 (2009) 383-390.
17. C. Oliva, L. Bonoldi, S. Cappelli, L. Fabbrini, I. Rossetti, L. Forni, J. Molec. Catal. A: Chemical, 226(1) (2005) 33-40.
18. L.Fabbrini, A.Kryukov, S.Cappelli, G.L.Chiarello, I.Rossetti, C.Oliva, L. Forni, J. Catal., 232(2) (2005) 247-256.
19. W.J. Stark, L. Mädler, S.E. Pratsinis, EP 1,378,489 A1 (2004) to ETH, Zurich, CH, 24 pp..
20. R. Strobel, S.E. Pratsinis, J. Mater. Chem., 17 (2007) 4743-4756.
21. T. Hinklin, B. Toury, C. Gervais, F. Babonneau, J.J. Gislason, R.W. Morton, R.M. Laine, Chem. Mater., 16 (2004) 21-30.
22. G.L. Chiarello, I. Rossetti, L. Forni, J. Catal., 236 (2005) 251-261.
23. G.L. Chiarello, I. Rossetti, L. Forni, P. Lopinto, G. Migliavacca, Appl. Catal. B: Environmental, 72 (2007) 218-226 (part 1), 227-232 (part 2).
24. G.L. Chiarello, I. Rossetti, P. Lopinto, G. Migliavacca, L. Forni, Catal. Today, 117 (2006) 549-553.
25. Selected Powder Diffraction Data, Miner. DBM (1-40), J.C.P.D.S., Swarthmore, PA, 1974-1992.
26. A.C Larson, R.B. Von Dreele, General Structure Analysis System (GSAS) (Los Alamos National Laboratory Report LAUR, 2004), p. 86.
27. B.H Toby, J. Appl. Cryst., 34 (2001) 210-213.
28. G. Thornton, B.C. Tofield, A.H. Hewat, J. Sol. State Chem., 61 (1986) 301-307.
29. E. Campagnoli, A. Tavares, L. Fabbrini, I. Rossetti, Yu. A. Dubitski, A. Zaopo, L. Forni, Appl. Catal. B: Environmental, 55(2) (2005) 133-139.
30. V. Szabo, M. Bassir, A. Van Neste, S. Kaliaguine, Appl. Catal. B: Environmental, 37 (2002) 175-180.

31. H. Arai, T. Yamada, K. Eguchi, T. Seiyama, Appl. Catal., 26 (1986) 265-276.
32. M.A. Peña, J.L.G. Fierro. Chem. Rev., 101 (2001) 1981-2017.
33. C. Batiot-Dupeyrat, F. Martinez-Ortega, M. Ganne, J.M. Tatibouët, Appl. Catal. A: General, 206 (2001) 205-215.
34. X.E. Verykios, F.P. Stein, R.W. Coughlin, Catal. Rev.-Sci. Eng., 22 (1980) 197-234.
35. H.A. Engelhardt, D. Menzel, Surf. Sci., 57 (1976) 591-618.
36. K.C. Prince, A.M. Bradshaw, Surf. Sci. 126 (1983) 49-57.
37. K.L. Anderson, J.K. Plischke, M.A. Vannice, J. Catal., 128 (1991) 148-160.
38. L. Kundakovic, M. Flytzani-Stephanopoulos, Appl. Catal. A: General, 183 (1999) 35-51.

TABLES

Table 1. Main catalyst properties. SSA = specific surface area (BET). Crystal size determined from XRD analysis. n.d. = not determined due to poor or lacking reflections.

Sample		SSA, m^2/g	Average crystal size, nm	Average Ag crystal size, nm
$LaCoO_3$	FP	43	-	-
$LaCoO_3$	SG (S0)	8	26	-
$LaCoO_3$	SG (S1)	7	16	-
$LaCoO_3$	SG (S2)	8	16	-
$La_{0.95}Ag_{0.05}CoO_3$	FP	44	9	3
$La_{0.95}Ag_{0.05}CoO_3$	SG	5	40	n.d.
$La_{0.9}Ag_{0.1}CoO_3$	FP	50	7	3
$La_{0.9}Ag_{0.1}CoO_3$	SG	7	32	5
$La_{0.8}Ag_{0.2}CoO_3$	FP	53	6	6
$La_{0.8}Ag_{0.2}CoO_3$	SG	3	33	4
2%Ag/$LaCoO_3$	SG	7	28	n.d.
5%Ag/$LaCoO_3$	SG	6	23	10
10%Ag/$LaCoO_3$	SG	3	31	8

Table 2. Activity data of fresh and poisoned catalysts (after 4 poisoning cycles). T_0= temperature at which CH_4 conversion started; T_{50}= temperature of 50% CH_4 conversion; $Conv_{450°C}$= CH_4 % conversion at 450°C. Activity data for poisoned samples given as CH_4 % conversion at 450°C. Δ = activity loss due to poisoning (conversion of fresh sample – residual after last poisoning cycle) expressed in points %.

Sample	Method	Fresh catalyst		Poisoned catalyst		Δ, %
		T_{50}	$Conv_{450}$,%	I cycle $conv_{450}$, %	Last cycle, $conv_{450}$, %	
$LaCoO_3$	FP	450	50	43.0	35.7	14.3
$LaCoO_3$(S0)	SG	490	30	22.9	17.5	12.5
$LaCoO_3$(S1)	SG	477	35	27.7	13.7	21.3
$LaCoO_3$(S2)	SG	484	34	26.5	20.8	13.2
$La_{0.95}Ag_{0.05}CoO_3$	FP	457	44.5	32.3	29.1	15.4
$La_{0.95}Ag_{0.05}CoO_3$	SG	456	46.9	45.0	35.9	11
$La_{0.9}Ag_{0.1}CoO_3$	FP	480	32.9	22.5	21.3	11.6
$La_{0.9}Ag_{0.1}CoO_3$	SG	482	33.2	22.7	25.8	7.4
$La_{0.8}Ag_{0.2}CoO_3$	FP	435	58.6	47.3	40.6	18
$La_{0.8}Ag_{0.2}CoO_3$	SG	480	36.6	17.2	16.7	19.9
2%Ag/$LaCoO_3$	SG	467	40.0	34.8	23.2	16.8
5%Ag/$LaCoO_3$	SG	454	48.4	47	28.5	19.9
10%Ag/$LaCoO_3$	SG	470	38.7	36.4	29	9.7

Table 3. Kinetic constant of methane combustion at 450°C.

Sample	Method	$k_m^{450}, \frac{\mu mole}{s \cdot g \cdot atm}$
$LaCoO_3$	FP	123
$LaCoO_3$(S0)	SG	61
$LaCoO_3$(S1)	SG	74
$LaCoO_3$(S2)	SG	71
$La_{0.95}Ag_{0.05}CoO_3$	FP	101
$La_{0.95}Ag_{0.05}CoO_3$	SG	101
$La_{0.9}Ag_{0.1}CoO_3$	FP	68
$La_{0.9}Ag_{0.1}CoO_3$	SG	70
$La_{0.8}Ag_{0.2}CoO_3$	FP	151
$La_{0.8}Ag_{0.2}CoO_3$	SG	72
2%Ag/$LaCoO_3$	SG	84
5%Ag/$LaCoO_3$	SG	114
10%Ag/$LaCoO_3$	SG	84

Table 4. Average deactivation rate (Torr/min; 1 Torr = 133 Pa) during each poisoning cycle [16].

Catalyst	Preparation method	Cycle 1	Cycle 2	Cycle 3	Cycle 4
$LaCoO_3$	FP	0.00092	0.0034	0.0066	0.0039
$LaCoO_3$ (S0)	SG	0.0068	0.01	0.0017	0.0027
$LaCoO_3$ (S1)	SG	0.0059	0.0004	-0.0039	0.0055
$LaCoO_3$ (S2)	SG	0.0032	0.00074	0.00075	-0.012
$La_{0.95}Ag_{0.05}CoO_3$	FP	0.01	0.0024	0.006	0.0055
$La_{0.95}Ag_{0.05}CoO_3$	SG	0.0027	0.0018	0	0.0071
$La_{0.9}Ag_{0.1}CoO_3$	FP	0.007	0.0024	-0.001	-0.0017
$La_{0.9}Ag_{0.1}CoO_3$	SG	0.0027	0.046	0.025	0.0016
$La_{0.8}Ag_{0.2}CoO_3$	FP	0.012	-0.0033	0	0.002
$La_{0.8}Ag_{0.2}CoO_3$	SG	0.0013	0.0044	0.0022	-0.0005
2%Ag/$LaCoO_3$	SG	0.0068	0.009	0.008	0.0065
5%Ag/$LaCoO_3$	SG	0.0075	0.0073	0.0023	0.006
10%Ag/$LaCoO_3$	SG	0.014	0.012	0.014	0.01

FIGURE CAPTIONS

Fig. 1: XRD patterns of *a*) FP samples: (1) Ag x=0.05, (2) Ag x=0.1, (3) Ag x=0.2; *b*) SG samples: (1) Ag x=0.05, (2) Ag x=0.1, (3) Ag x=0.2; *c*) Supported samples: (1) Ag 2 wt%, (2) Ag 5 wt%, (3) Ag 10 wt%. (■) Perovskitic phase, (□) metallic Ag phase, (*) unknown impurity.

Fig.2: Rietveld refinement of XRD profiles. *a*) example of fitting of FP-prepared $LaCoO_3$; b) cell volume dependence on Ag-doping: full symbols FP samples, empty symbols SG ones. Insert: experimentally determined Ag wt% in extraframework position (E.F.) *vs*. nominal composition expressed coherently.

Fig. 3: Catalytic activity of undoped, fresh $LaCoO_3$ catalysts: (■) FP, (▲) SG-S0, (♦) SG-S1, (●) SG-S2.

Fig. 4: Comparison between cell volume (full symbols) and catalytic activity (empty symbols) for SG (*a*) and FP (*b*) samples.

Fig 5: Catalytic activity of fresh SG $La_{1-x}Ag_xCoO_3$ catalysts (■) $La_{0.95}Ag_{0.05}CoO_3$, (▲) $La_{0.9}Ag_{0.1}CoO_3$, (♦) $La_{0.8}Ag_{0.2}CoO_3$, (●) $LaCoO_3$

Fig. 6: Catalytic activity of fresh FP $La_{1-x}Ag_xCoO_3$ catalysts (■) $La_{0.95}Ag_{0.05}CoO_3$, (▲) $La_{0.9}Ag_{0.1}CoO_3$, (♦) $La_{0.8}Ag_{0.2}CoO_3$, (●) $LaCoO_3$

Fig. 7: Catalytic activity of fresh SG catalysts x%Ag/$LaCoO_3$ (post synthesis Ag loading) (■) $LaCoO_3$, (▲) 10%Ag/$LaCoO_3$, (♦) 5%Ag/$LaCoO_3$, (●) 2%Ag/$LaCoO_3$.

Fig. 8 Temperature Programmed Reduction pattern of selected samples: thin dotted line FP-$LaCoO_3$; thick dotted line FP-$La_{0.95}Ag_{0.}$05CoO3; continuous black line SG-$La_{0.8}Ag_{0.2}CoO_3$; continuous thick grey line SG-$La_{0.95}Ag_{0.}$05CoO3.

Fig. 9: Catalytic activity after sulphur poisoning of SG samples (after IV cycle): (■) $La_{0.95}Ag_{0.05}CoO_3$, (▲) $La_{0.9}Ag_{0.1}CoO_3$, (♦) $La_{0.8}Ag_{0.2}CoO_3$, (●) $LaCoO_3$.

Fig. 10: Catalytic activity after sulphur poisoning of FP-prepared materials (after IV cycle): (■) $La_{0.95}Ag_{0.05}CoO_3$, (▲) $La_{0.9}Ag_{0.1}CoO_3$, (♦) $La_{0.8}Ag_{0.2}CoO_3$, (●) $LaCoO_3$.

Fig. 11: Catalytic activity after sulphur poisoning of post-synthesis functionalised catalysts (after IV cycle): (■) $LaCoO_3$, (▲) 10%Ag/$LaCoO_3$, (♦) 5%Ag/$LaCoO_3$, (●) 2%Ag/$LaCoO_3$.

Scheme 1: summary of the possibile effect of Ag doping on catalytic activity.

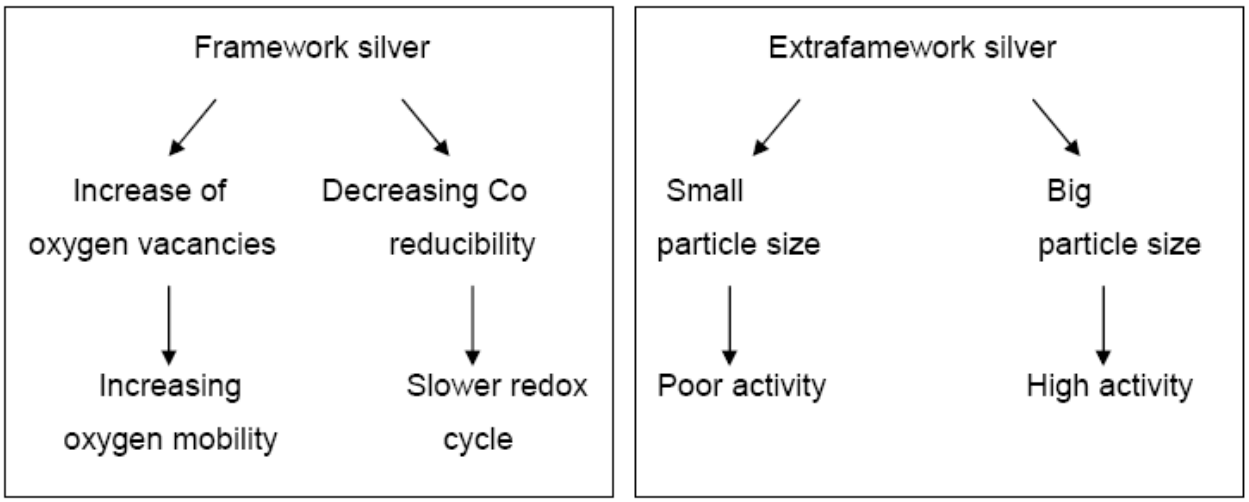

Fig. 1a

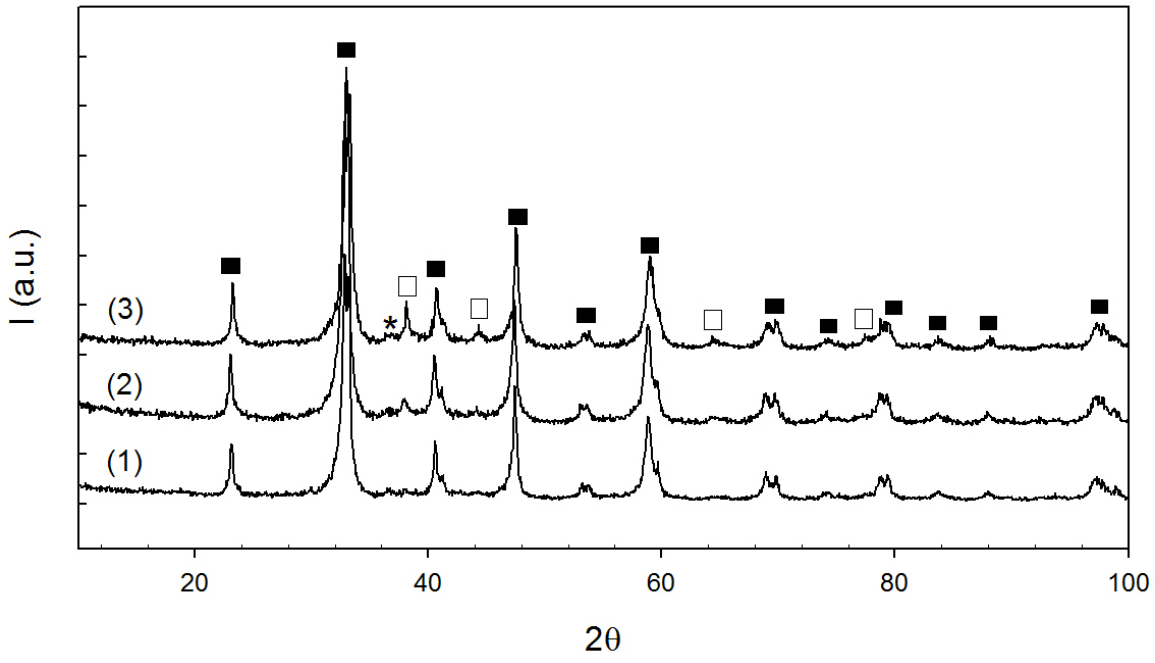

Fig. 1b

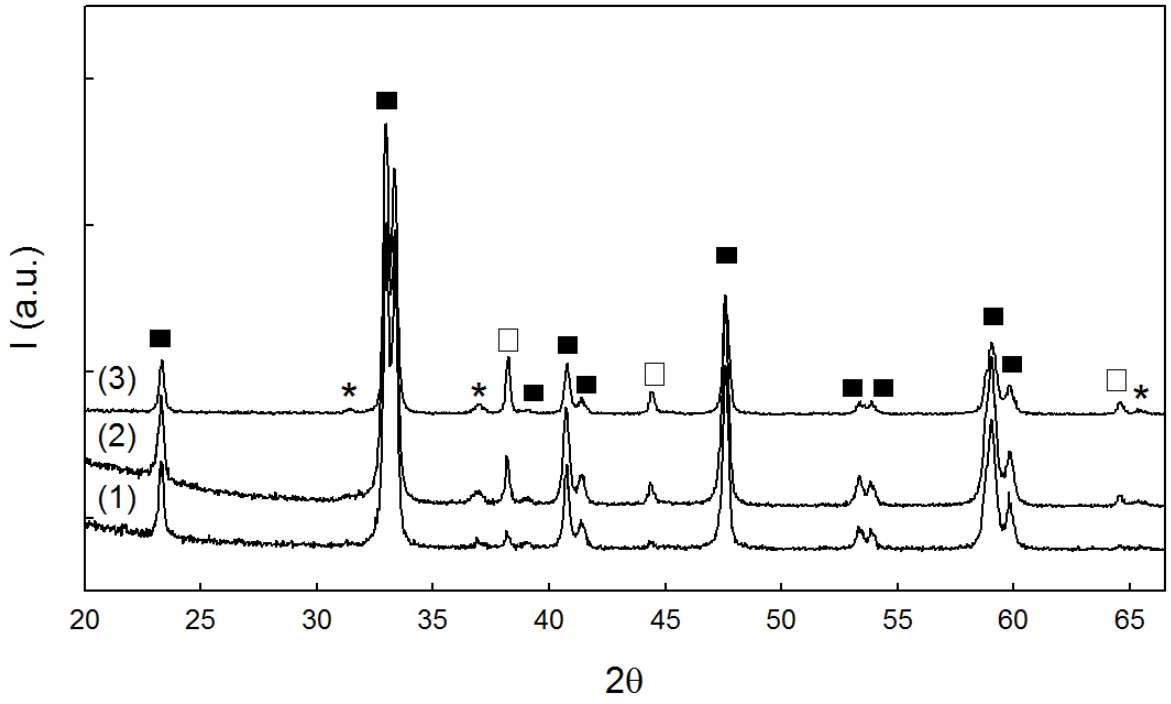

Fig. 1c

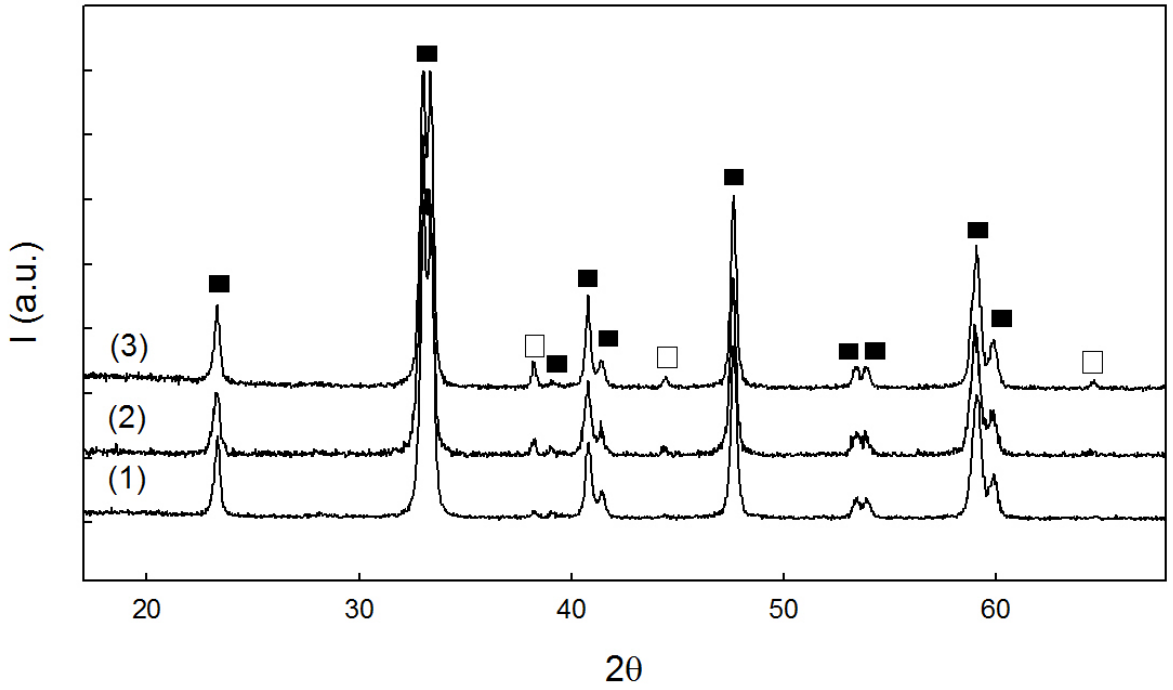

Fig. 2a

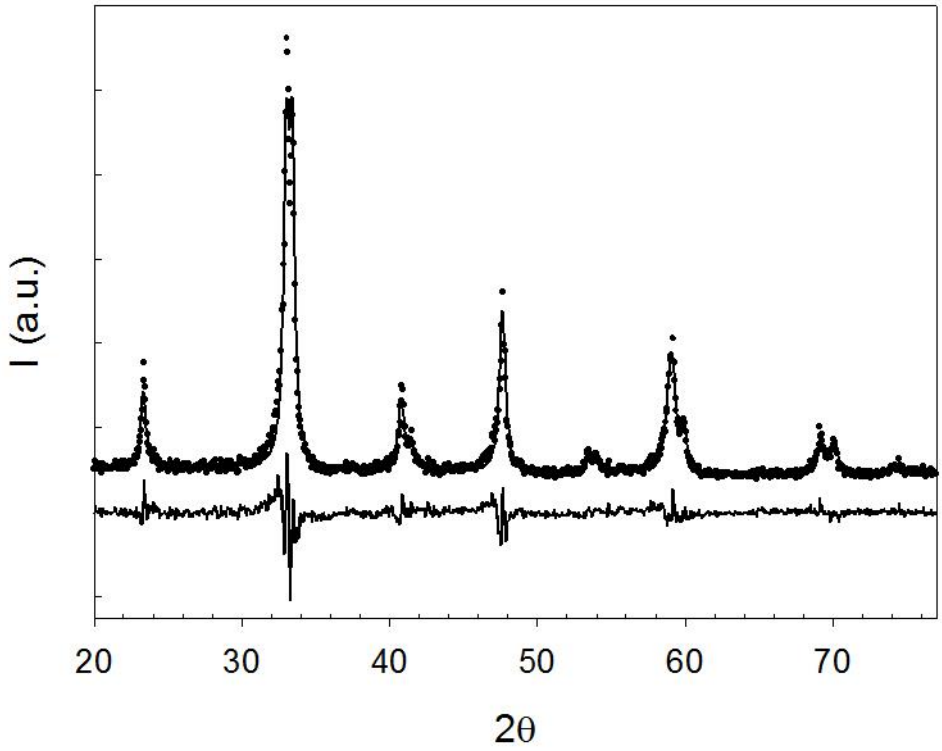

Fig. 2b

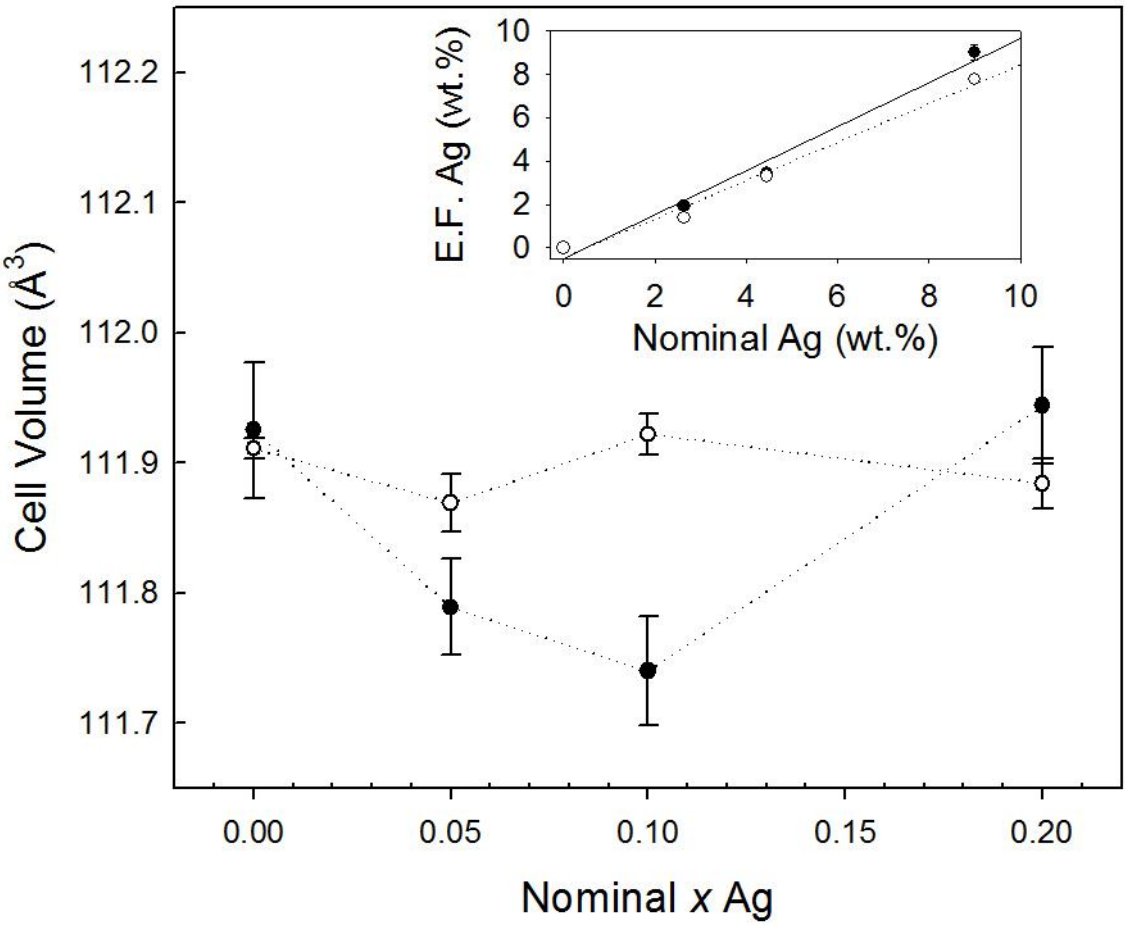
Cell Volume (Å^3)
112.2
112.1
112.0
111.9
111.8
111.7
0.00
0.05
0.10
0.15
0.20
Nominal *x* Ag
E.F. Ag (wt.%)
0
2
4
6
8
10
Nominal Ag (wt.%)

Fig. 3

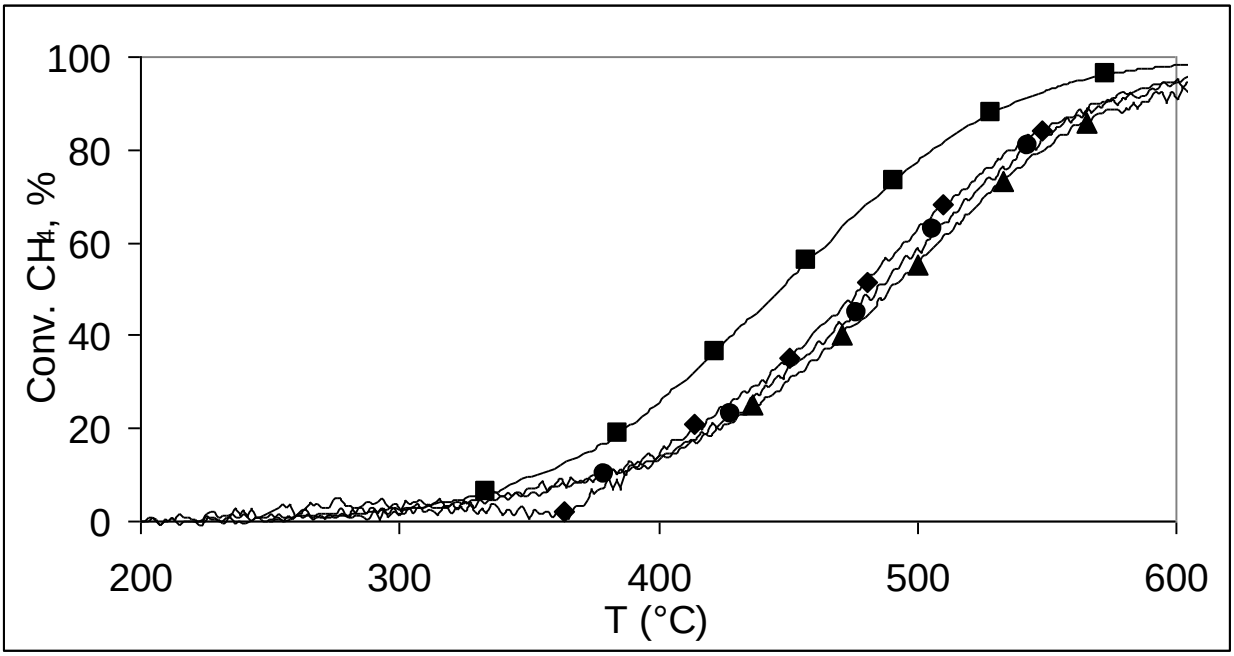
Conv. CH$_4$, %
0
20
40
60
80
100
200
300
400
500
600
T (°C)

Fig. 4a

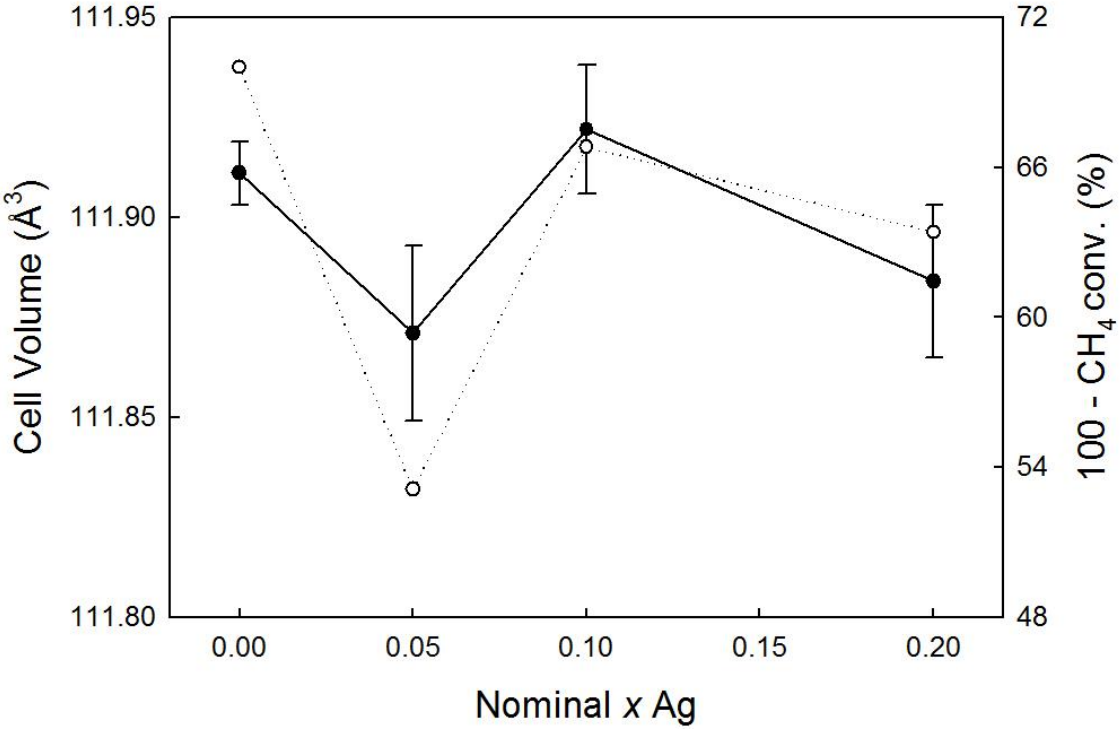
111.95
111.90
111.85
111.80
Cell Volume (Å^3)
72
66
60
54
48
100 - CH_4 conv. (%)
0.00
0.05
0.10
0.15
0.20
Nominal *x* Ag

Fig. 4b

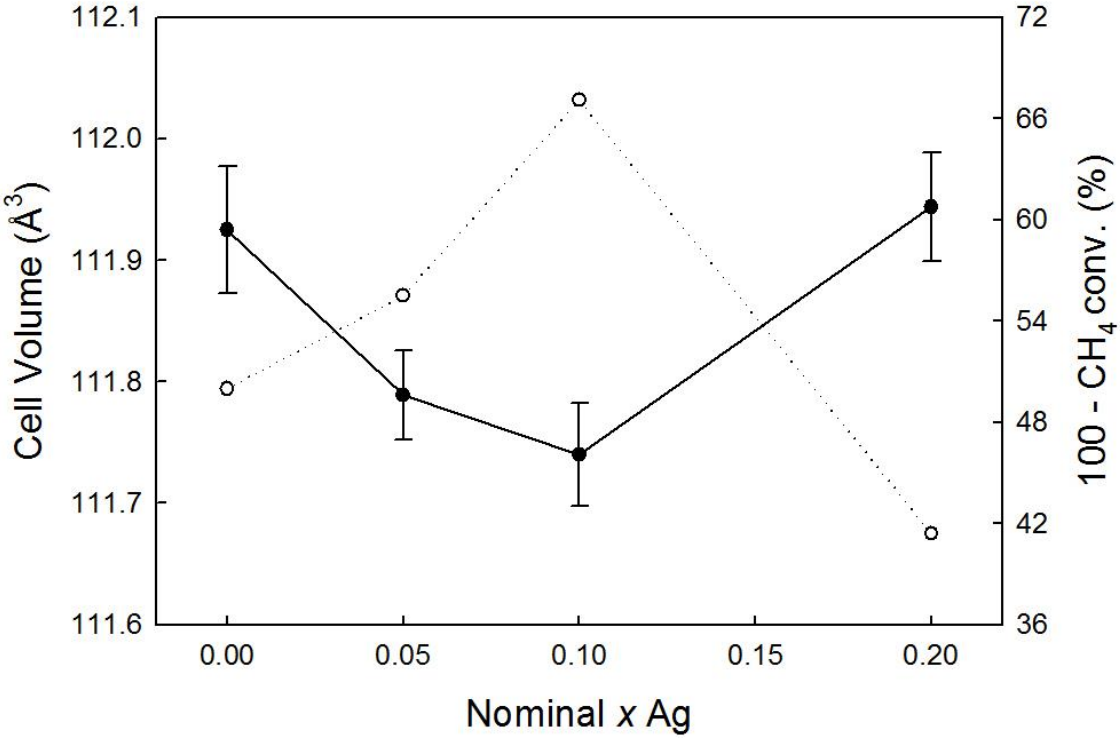
112.1
112.0
111.9
111.8
111.7
111.6
Cell Volume (Å^3)
72
66
60
54
48
42
36
100 - CH_4 conv. (%)
0.00
0.05
0.10
0.15
0.20
Nominal *x* Ag

Fig.5

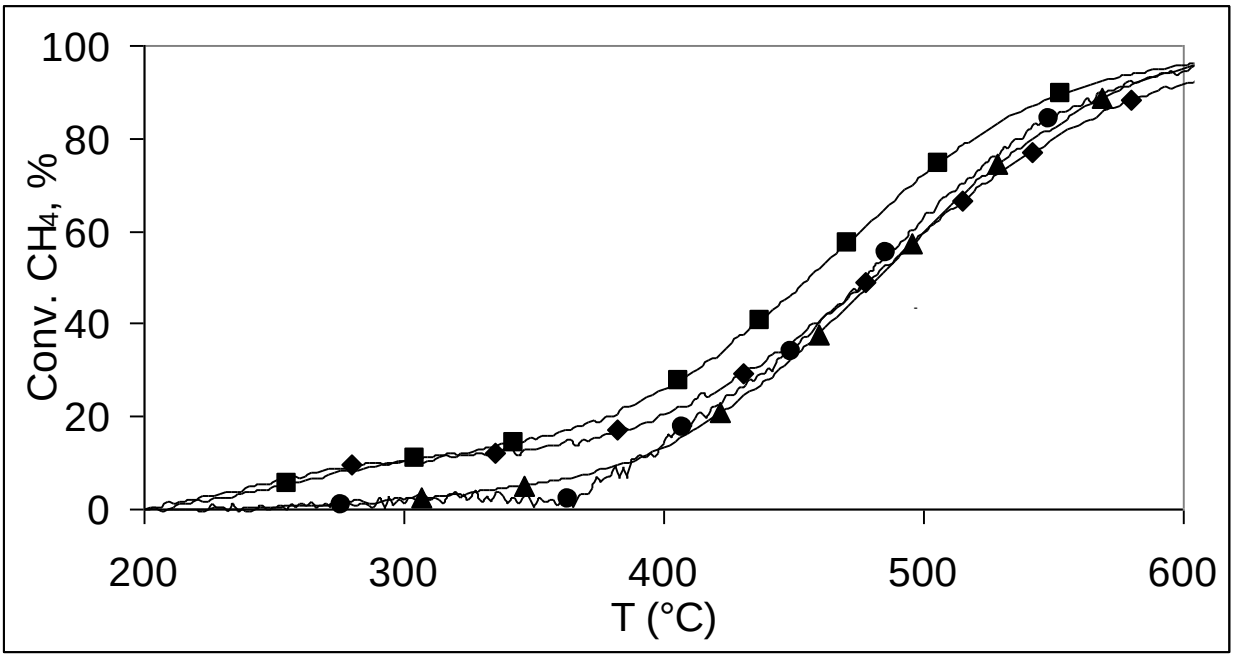
100
80
60
40
20
0
Conv. CH4, %
200
300
400
500
600
T (°C)

Fig. 6.

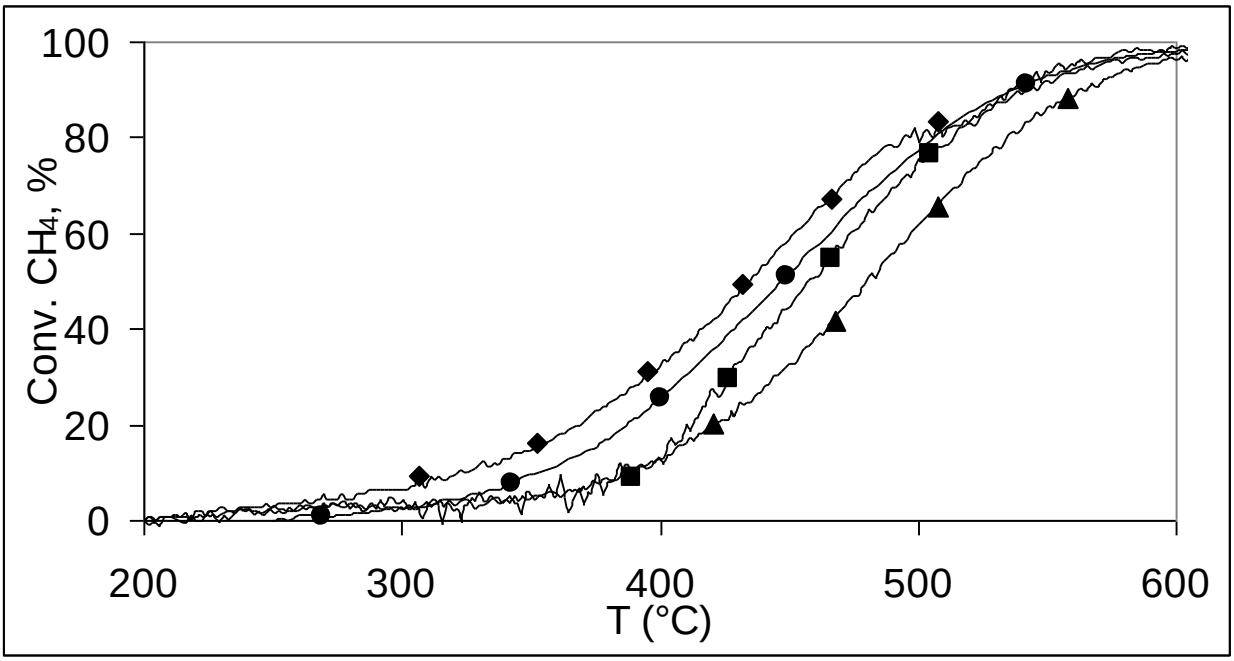
100
80
60
40
20
0
Conv. CH4, %
200
300
400
500
600
T (°C)

Fig. 7.

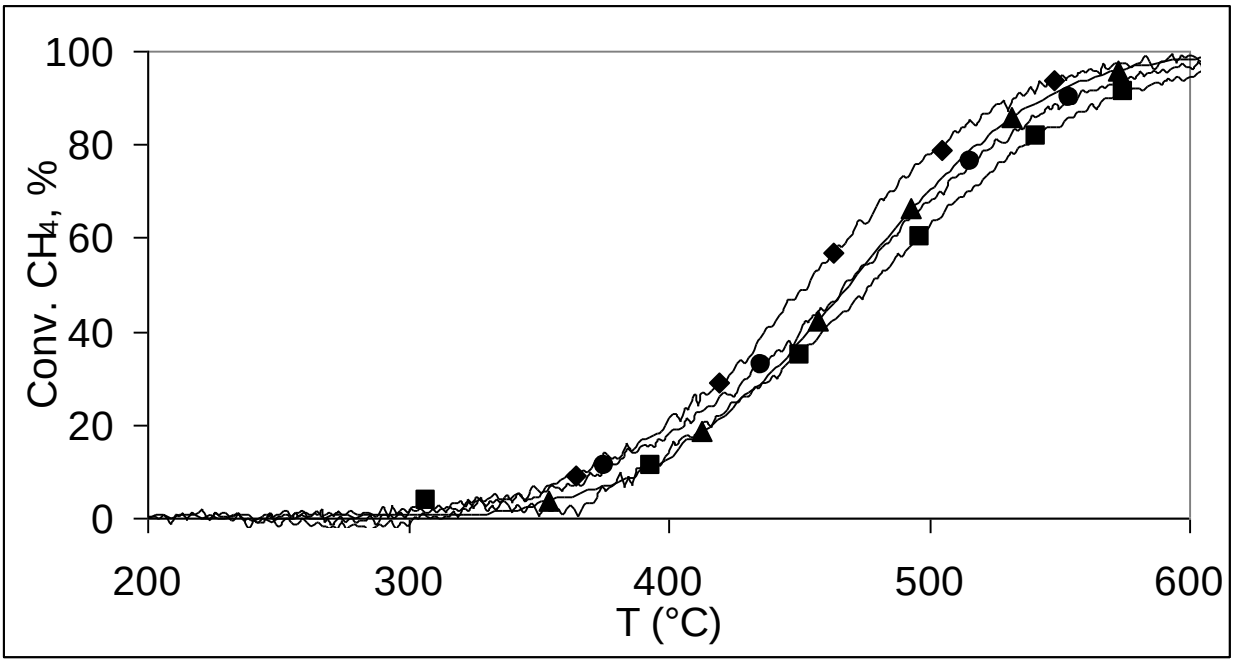
100
80
60
40
20
0
Conv. CH4, %
200
300
400
500
600
T (°C)

Fig.8

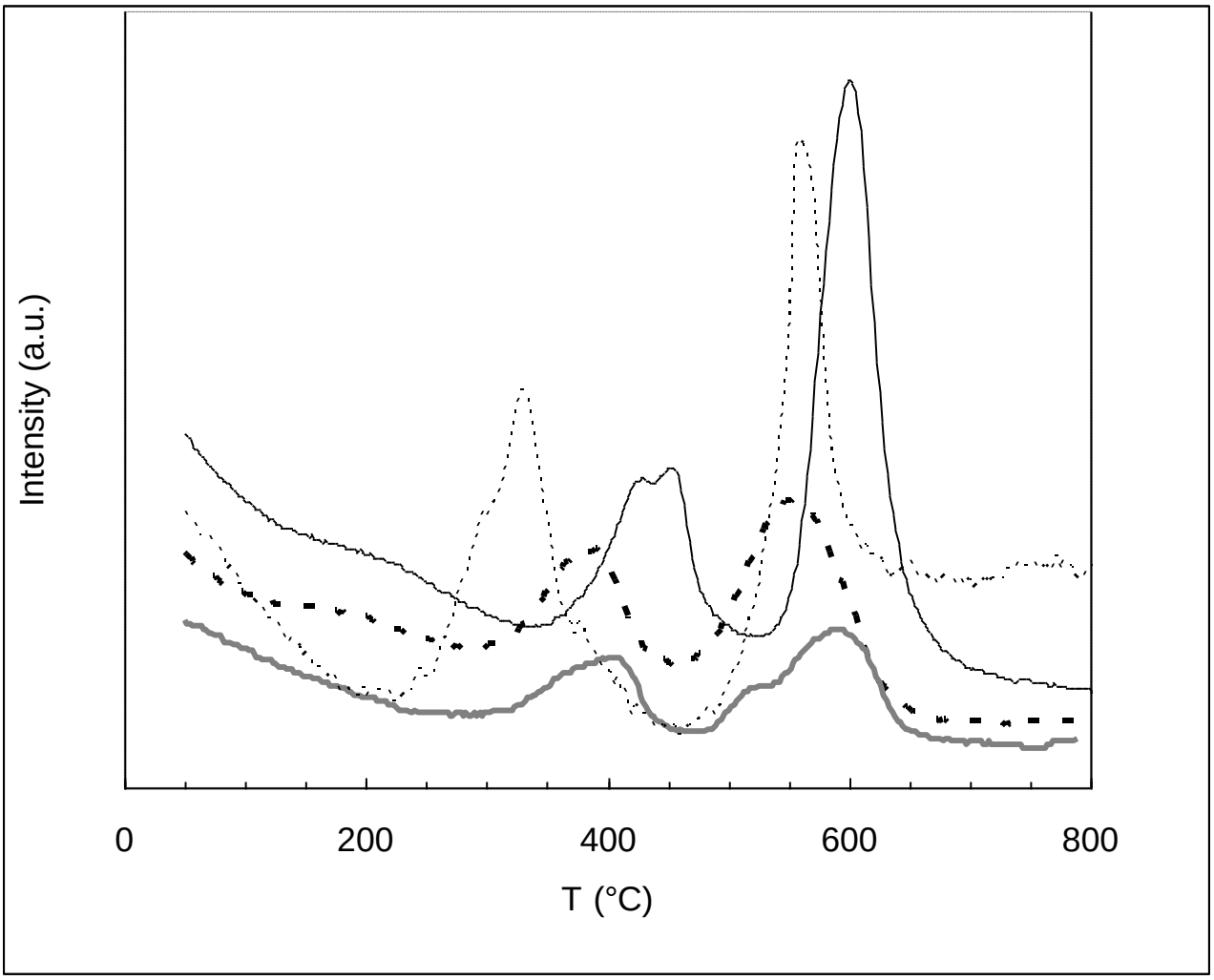
Intensity (a.u.)
0
200
400
600
800
T (°C)

Fig. 9

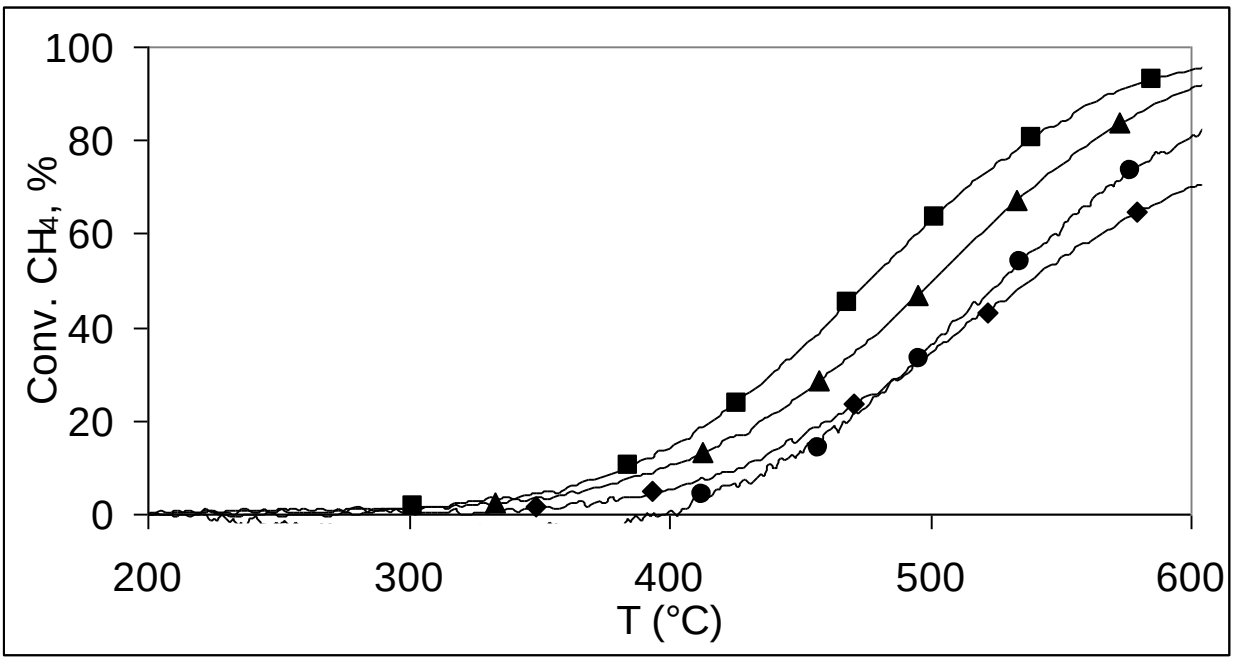
100
80
60
40
20
0
Conv. CH4, %
200
300
400
500
600
T (°C)

Fig. 10

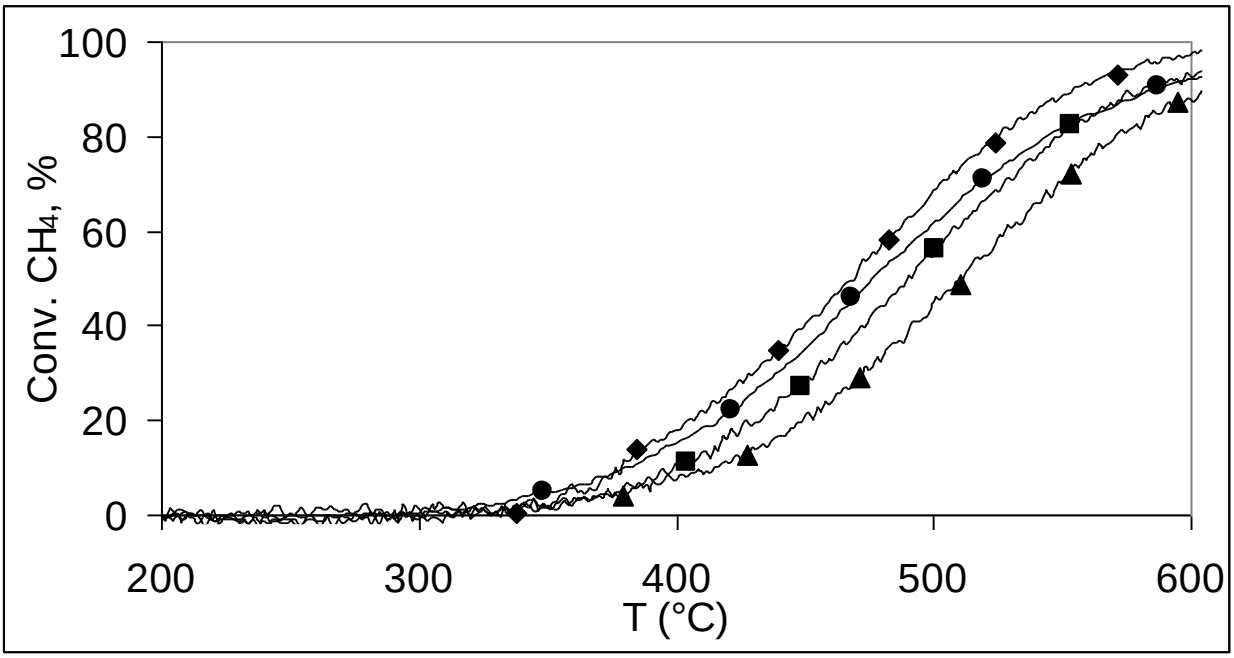
100
80
60
40
20
0
Conv. CH4, %
200
300
400
500
600
T (°C)

Fig. 11